TELOMERIC DOUBLE STRAND BREAKS FACILITATE FORMATION OF 5' C-RICH OVERHANGS IN G1 HUMAN CELLS

Christopher B Nelson[1,2,1], Taghreed Alturki[1,2], Lynn Taylor[2], David G Maranon[2], Keiko Muraki[3], John P. Murnane[3], and Susan M Bailey[1,2*]

[1]Cell and Molecular Biology Program and [2]Department of Environmental and Radiological Health Sciences, Colorado State University, Fort Collins, CO

[3]Department of Radiation Oncology, University of California, San Francisco, CA.

Keywords: Telomeres; Telomere DSBs; C-rich telomeric overhangs; G1 human cells

[†] Present address: Children's Medical Research Institute, 214 Hawkesbury Road, Westmead NSW, 2145, Australia

* Corresponding author. Email address: Susan.Bailey@colostate.edu

Abstract

Telomeres are repetitive nucleoprotein complexes that protect the ends of linear chromosomes and prevent their detection as double strand breaks (DSBs), thereby averting activation of a DNA damage response (DDR). While these functions are clearly essential for maintaining genome integrity, it is intriguing to consider how DSBs within telomeres themselves are handled. In cycling cells, telomeric DSBs can be repaired by homologous recombination (HR) and alternative nonhomologous end-joining (ALT NHEJ). Localization of 53BP1, an important regulator of resection at broken ends, to damaged telomeres has also only been observed in replicating cells. Here, we characterized the cellular response to enzymatically induced telomeric DSBs, specifically in non-replicating G1 normal human fibroblasts and cancer cells. Telomeric DSBs in G1 human cells elicited early signatures of a DDR in that gamma (γ)-H2AX and MDC1 were recruited to broken telomeres. Consistent with previous reports, 53BP1 was not observed at telomeric break sites in G1. Furthermore, evidence of classical NHEJ (cNHEJ), the primary pathway of DSB repair in G1 mammalian cells, was lacking at broken telomeres. Likewise, no evidence of classical HR-dependent repair of telomeric DSBs in G1 was observed, as neither RAD51, RAD52, nor repair associated DNA synthesis were detected. Rather, and consistent with rapid truncation events and overall telomere shortening, telomeric DSBs in G1 human cells facilitated formation of extensive tracks of RPA coated 5' C-rich telomeric single-stranded (ss)DNA, an observation also supported by minimal dependence on conventional end-processing exonucleases MRE11, EXO1, or Apollo. Thus, telomeric DSBs in G1 human cells initiate an abbreviated DDR that results in extensive resection in the absence of 53BP1, facilitating formation of 5' C-rich overhangs, a previously proposed marker of the recombination dependent, alternative lengthening of telomeres (ALT) pathway, which presumably persist until recombination-mediated elongation and restoration is possible.

INTRODUCTION

Telomeres, specialized nucleoprotein complexes that "cap" the ends of linear chromosomes, are composed of highly conserved, G-rich tandem repeats [$(5'\text{-TTAGGG-}3')_n$ in vertebrates] (1). Telomeres end with a 3' single-stranded (ss) G-rich overhang (2), which serves as the substrate for telomerase mediated synthesis of telomeric DNA (3). Telomerase is the reverse transcriptase capable of maintaining telomere length via RNA template-dependent addition of telomeric repeats onto the ends of newly replicated chromosomes. Telomerase activity is prominent in highly proliferative populations like germ-line, stem, and the vast majority of cancer cells, thereby endowing them with extended or unlimited replicative potential (4, 5). The remaining ~10% of human cancers maintain telomere length via a recombination dependent, alternative lengthening of telomeres (ALT) mechanism (6) that display a number of defining features, including heterogeneous telomere lengths, increased frequencies of telomere sister chromatid exchange (T-SCE), ALT-associated PML bodies (APBs), and extrachromosomal telomeric repeats (ECTR), which include C-rich ss circles (C-circles) (7-10).

The G-rich telomeric 3' ss overhang is also required for the formation of protective terminal structural features termed t-loops (11). Telomeres are bound by shelterin, a six-member telomere-specific protein complex that contributes to the regulation of telomerase activity, t-loop formation, and protection of chromosome ends (12). Functional telomeres are essential for maintaining genome stability, as they protect natural chromosomal termini from degradation and prevent them from being recognized as double strand breaks (DSBs) and triggering of an inappropriate DNA damage response (DDR) (13-16). Inhibition of conventional repair activities at telomeres has been demonstrated (15, 17-19), raising the question of how – and even whether – DSBs occurring within telomeric repeats themselves are repaired. Various strategies employing targeted enzymatic cleavage of telomeric repeats have recently enabled studies to directly address this issue (20-23).

Enzymatically induced telomeric DSBs in murine cells have been shown to activate a DDR and recruitment of p53 binding protein 1 (53BP1) in a subpopulation of cycling cells, specifically those undergoing DNA replication (23). Moreover, homologous recombination (HR) and alternative non-homologous end joining (alt-NHEJ), but not classical NHEJ (c-NHEJ), occur following induction of telomeric DSBs in cycling cell populations (22, 23). These results suggest that while repair of telomeric DSBs is possible, it may be limited to cells undergoing replication. Such a notion is also supported by studies utilizing global DNA damaging agents – ionizing radiation (IR) and hydrogen peroxide – which although would only rarely be expected to directly produce prompt telomere-specific DSBs, have shown that telomeric damage responses persist in G1 cells that undergo senescence (24, 25).

Whether or not repair of telomeric DSBs requires cell cycle progression (i.e., replication) has physiological relevance, as many human adult tissues are largely post-mitotic and unrepaired DSBs can trigger senescence, thereby contributing to degenerative pathologies (24, 25). Here, we investigated human cellular responses to targeted telomeric DSBs specifically in G1 utilizing the telomere-specific endonuclease TRAS1-EN-TRF1 (EN-T) (20, 21). Signatures of an early DDR were observed, as gamma (γ)–H2AX and mediator of DNA damage checkpoint protein 1 (MDC1) foci co-localized with broken telomeres. However, and consistent with previous reports, 53BP1 was not recruited to telomeric DSBs in G1 (23).

Due to the scarcity of a homologous template, NHEJ is regarded as the primary DSB repair pathway during G1 in mammalian cells (26-28). Here, both short hairpin (sh)RNA depletion and chemical inhibition of the key NHEJ kinase, DNA-dependent protein kinase catalytic subunit (DNA-PKcs), suggested that cNHEJ was not a major contributor to repair of telomeric DSBs in G1 human cells. Likewise, no evidence of classical HR-dependent repair of telomeric DSBs in G1 was found, as neither RAD51, RAD52 (early responders that promote and stimulate strand invasion, respectively), nor repair associated DNA synthesis were detected.

The most striking observation at telomeric DSBs in G1 were extensive tracks of predominantly 5' C-rich ss telomeric DNA, which co-localized with Replication Protein A (RPA). Interestingly, S4/S8 phosphorylated RPA (pRPA) foci, which are associated with activation of RPA during DNA repair (29), had only modest dependence on the conventional end processing exonucleases MRE11 (3'-to-5') and EXO1 (5'-to-3'). The 5'-to-3' nuclease Apollo, which has been implicated in post-replicative processing specifically of leading-strand telomeres (30), also did not influence resection at telomeric DSBs in G1.

Taken together, our results support the view that telomeric DSBs in G1 human cells represent rapid truncation events, in that they are associated with telomere shortening and facilitate formation of 5' C-rich overhangs, previously proposed markers of the recombination and replication-dependent ALT pathway of telomere maintenance (31). We propose that enrichment of 5' C-rich overhangs results from telomere DSB-mediated deletion of protective t-loops in G1 and extensive resection in the absence of 53BP1, and further, that such structures, although presumably unstable unless protected, persist into S/G2 for replication/HR dependent ALT processing and elongation into functional telomeres as a means of repair.

RESULTS

Characterization of targeted telomeric DSBs in human G1 cells

To better understand human cellular responses to telomeric DSBs throughout the cell cycle, we performed transient transfection experiments using a plasmid encoding a flag-tagged telomere repeat-specific endonuclease fused to the human TRF1 gene (TRAS1-EN-TRF1: hereafter referred to as EN-T) that produces blunt ended DSBs within telomeres (20, 21). For experiments involving EN-T, several human cell lines were selected. U2OS cells (ALT, telomerase independent, phenotype) served as a positive control for EN-T activity as ALT cells

undergo recombinational repair at telomeric DSBs. BJ1 hTERT immortalized fibroblasts (telomerase positive) were also chosen, as they represent a relatively normal, non-tumorigenic human cell line. Lastly, EJ-30, a bladder carcinoma cell line, was employed (highly telomerase positive), as they have been used extensively to study sub-telomeric DSB repair (32-34).

Following transient transfection of EN-T or Flag-TRF1, co-localization with telomeres was observed in all cell lines (**Supp Fig 1A**). Evidence of DSB signaling following EN-T expression in EJ-30 (non-ALT) cells was also evaluated, which included phosphorylation of ATM (S1981) and CHK2 (Thr68) (**Supp Fig 1B**). Transfection alone induced some DSB signaling activity, noted by the modest increase in intensity of phospho-ATM and phospho-CHK2 bands in TRF1 transfected samples relative to no treatment controls. Supportive of telomere cutting, a decrease in Telomere Restriction Fragment (TRF) size was observed following EN-T expression, as compared to TRF1 and untransfected controls (**Supp Fig 1C, D**). EN-T expression reduced the mean TRF by ~ 5-10%, consistent with expectation considering the relatively low transfection efficiency in EJ-30 cells (~20-30%), and that not all telomeres were broken (~8-12/cell).

To further validate the EN-T system, we sought to reproduce the finding that induced telomeric DSBs stimulate a damage response and repair via some combination of HR and break-induced replication (BIR) in ALT cells (35, 36). ALT U2OS cells exhibited activation of telomere damage responses upon transfection with EN-T as expected, and as evidenced by increased γ-H2AX foci compared to untransfected cells; a significant portion of these damage responses were found to occur at broken telomeres, as γ-H2AX foci colocalized (overlapped) with EN-T foci (**Supp Fig 2A**). Additionally, following EN-T transfection, U20S cells harbored elevated levels of RAD51 and RAD52-YFP foci, mediators of HR and BIR respectively, which frequently colocalized with EN-T foci, confirming repair of telomeric DSBs by HR and BIR in cycling human ALT cells (**Supp Fig 2B, C**).

As various lines of evidence have suggested that DSB repair may be non-conventional or even non-existent within or near telomeres of normal cells in G1 phase (22-25), we sought to investigate damage responses and repair of broken human telomeres in G1 directly. In order to study telomeric DSBs specifically in G1 non-ALT EJ-30 (telomerase positive; cancer) cycling cells, we developed a DAPI intensity-based approach as a means of distinguishing cell cycle phases in interphase nuclei, which retained the ability to make accurate measurements of fluorescent foci. Cells in G1 form a clear peak in the lower intensity portion of a DAPI intensity histogram using even a relatively low number (~300) of cells (**Supp Fig 3A**). The specificity of the G1 DAPI intensity peak was validated via exclusion of Cyclin A, which stains S and G2 cells. A similar DAPI intensity histogram was generated to distinguish G1 from S/G2 in all imaging experiments involving EJ-30 cells. Reliable discrimination between S and G2 could not be achieved with this approach, therefore these populations were pooled throughout analyses.

Telomeric DSBs in essentially normal BJ1 hTERT G1 cells were also evaluated. Transfection efficiency in BJ1 hTERT cells with either EN-T or TRF1 was quite low (0.5-2% of cells), and only a very small percentage of transfected cells stained positive for Cyclin A (EN-T: 0%, TRF1: 3.2%**, Supp Fig 3B**) or bromodeoxyuridine (BrdU; **Supp Fig 3C**), consistent with the vast majority of transfected BJ1 hTERT cells being in G1 phase 48 hr post transfection.

Non-canonical damage response at telomeric DSBs in G1 human cells lacks recruitment of 53BP1

To investigate damage responses at individual telomeric DSBs, we evaluated co-localization of γ-H2AX and 53BP1 foci at broken telomeres by immunofluorescence. Telomere-specific DSBs co-localized with γ-H2AX in BJ1 hTERT G1 cells ($p = 0.012$; **Fig 1A**), and in all phases of the cell cycle in EJ-30 cells ($p = 0.0009$ in G1 cells, 0.022 in S/G2 cells; **Fig. 1C**). Telomeric DSBs also co-localized with 53BP1 in EJ-30 S/G2 cells ($p = 0.012$); however, 53BP1

was not observed at broken telomeres in either BJ1 hTERT or EJ-30 G1 cells (**Fig 1B, D**). To determine whether other components of the early DNA damage response were initiated by telomeric DSBs in G1, we also evaluated MDC1, an early mediator of the response to genomic DSBs that acts downstream of γ-H2AX, but upstream of 53BP1 (37). MDC1 foci were induced to a similar degree as γ-H2AX in response to telomeric DSBs in BJ1 hTERT G1 cells ($p = 0.0007$, **Fig 2A**).

To determine whether other telomere DNA damaging methodologies produced similar results, we compared the intensity of γ-H2AX and 53BP1 foci co-localized at broken telomeres versus at random genomic sites that occurred within spatially defined stripes of damage generated by laser microirradiation. Consistent with our results using EN-T, 30 minutes after exposure of BJ1 HTERT cells, the intensity of γ-H2AX was found to be similar at telomeres and random sites within the microirradiation stripe, while the intensity of 53BP1 was reduced at broken telomeres compared to random sites ($p = 0.099$; **Fig 2B**).

Lastly, we reasoned that normal telomere protection activity might prevent recruitment of 53BP1 to broken telomeres. Therefore, a variety of strategies were employed to compromise telomeric end-protection, including relaxation of chromatin utilizing the histone deacetylase inhibitor Trichostatin A (or exposure to a hypotonic solution; not shown), partial depletion of the shelterin component telomere repeat factor 2 (TRF2) via small interfering (si)RNA knockdown (above the level that induces a damage response), as well as small hairpin (sh)RNA knockdown of shelterin-associated DNA-PKcs (**Supp Fig 4A-D)**. However, none of these conditions resulted in recruitment of 53BP1 to telomeric DSBs in G1 human cells**.** These results further support the finding that although telomeric DSBs in G1 activate an early DDR (γ-H2AX, MDC1 recruitment), they do not attract 53BP1 to break sites.

No evidence for cNHEJ at telomeric DSBs in G1 human cells

The absence of 53BP1 recruitment to telomeric DSBs in G1, particularly with shRNA knockdown of DNA-PKcs, suggested that cNHEJ may not be occurring (38-40). Autophosphorylation of DNA-PKcs at serine 2056 was slightly increased in EJ-30 cells expressing EN-T compared to cells expressing TRF1 or no treatment controls; ionizing radiation-induced DNA-PKcs autophosphorylation was prevented by treatment with the specific kinase inhibitor NU7026 (**Fig 3A**). We then tested whether DNA-PKcs autophosphorylation influenced telomere DSB repair in G1 by comparing TRF blots in cells expressing EN-T to those expressing EN-T and treated with NU7026 (**Fig 3B**). Chemical inhibition of DNA-PKcs autophosphorylation (NU7026, 24 hrs) in cycling EJ-30 cells expressing EN-T did not change the TRF size relative to control, again suggesting that cNHEJ does not significantly contribute to repair of telomeric DSBs in G1.

Telomeric DSBs in G1 are characterized by ssDNA, which is predominately 5' C-rich

We hypothesized that telomeric DSBs that fail to recruit 53BP1 may be particularly vulnerable to resection. To investigate the presence of ssDNA at telomeric DSBs in G1, fluorescence in situ hybridization (FISH) using a C-rich telomere probe – without denaturation of the DNA duplex (detects 3' G-rich ss telomeric DNA) – was performed in BJ1 hTERT G1 cells transfected with EN-T or TRF1. Indeed, telomeric ssDNA was more abundant in cells transfected with EN-T as compared with TRF1 transfection or no treatment controls ($p = 0.0002$, **Fig 4A**). To determine whether resection occurred bidirectionally, we also performed the ssFISH assay with a G-rich telomere probe (detects 5' C-rich ss telomeric DNA). Interestingly, hybridization with the G-rich probe produced many more signals overall, and more signals in EN-T transfected cells than in TRF1 transfected or no treatment controls ($p = 0.045$, **Fig 4B**). These results reveal that the telomeric ssDNA present at telomere-specific DSBs in G1 is enriched for 5' C-rich ss telomeric DNA.

To further validate the presence of ssDNA in cells transfected with EN-T, we immunostained for RPA70 and phospho-RPA32 (S4/S8). Following induction of telomeric DSBs, phospho-RPA32 showed pronounced and frequent colocalization with EN-T-flag in BJ1 hTERT G1 cells ($p = 0.0000046$ **Fig 5A**). Interestingly, RPA70 foci were not significantly increased by expression of EN-T ($p = 0.27$ **Fig 5B**). We observed similar increases in ss telomeric DNA and phospho-RPA32 in EJ-30 G1 cells expressing EN-T; as expected, this increase was also seen in S/G2 EJ-30 cells expressing EN-T (**Supp Fig 5B).**

ssDNA at telomeric DSBs in G1 is not dependent on conventional exonucleases, nor does it engage in homology dependent repair.

The presence of extensive tracks of ssDNA at telomeric DSBs in G1 suggested that long range resection was occurring. Therefore, we investigated the role of conventional end-processing exonucleases MRE11 (3'-to-5') and EXO1 (5'-to-3'), known mediators of resection at genomic DSB sites and at telomeres, respectively, in phospho-RPA foci induction following EN-T expression. Following chemical inhibition of MRE11 (via treatment with the small molecule inhibitor PFM01) in EN-T expressing BJ1 hTERT G1 cells, phospho-RPA32 foci were only slightly reduced compared to EN-T expressing controls ($p = 0.24$ **Fig 5C**). Phospho-RPA32 foci were also only slightly reduced when BJ1 hTERT cells were partially depleted of EXO1 (siRNA); the difference was not statistically significant ($p = 0.10$ **Fig 5C**). Thus, the majority of resection at telomeric DSBs in G1 human cells appears to occur independently of conventional resection machinery.

An alternative explanation for the presence of ssDNA at telomeric DSBs in G1 could be that it represents an attempt to regenerate a normal ss telomeric G-rich overhang for t-loop formation and end-protection (11). The SNM1B/Apollo (5'-to-3' exo) nuclease has been shown to be necessary for generation of the telomeric 3' G-rich overhang at blunt-ended leading-strand telomeres in mice (41, 42). Therefore, we hypothesized that Apollo may act bidirectionally at

telomeric DSBs, explaining the unexpected C-rich overhangs observed. However, EN-T-expressing Apollo$^{-/-}$ EJ-30 human cells exhibited only a slight reduction in C-rich ss telomeric foci in G1 compared to wild type (WT) cells ($p = 0.37$, **Supp Fig 5A**). Additionally, EN-T expressing Apollo$^{-/-}$ EJ-30 cells in G1 had more telomere phospho-RPA32 foci than EN-T expressing EJ-30 G1 WT cells ($p = 0.099$ **Supp Fig 5B**). Furthermore, both measures of telomeric ssDNA were slightly increased in the Apollo$^{-/-}$ S/G2 populations compared to WT cells. Thus, the Apollo nuclease is not responsible for the extensive resection observed at telomeric DSBs in G1 human cells.

To determine whether telomere DSB-induced resected ss telomeric DNA in G1 could represent an early element of HR dependent repair (for strand-invasion), we evaluated induction of RAD51 foci post EN-T transfection. While RAD51 foci were observed at telomeres in EN-T expressing EJ-30 S/G2 cells, they were *not* detected in EN-T expressing BJ1 hTERT or EJ-30 G1 cells (**Fig 6A**). Additionally, neither RAD52, nor repair associated DNA synthesis (BrdU incorporation) were detected following induction of telomeric DSBs in BJ1 hTERT G1 cells (**Fig 6B; Supp Fig 3C**). Taken together, these results indicate that telomeric ssDNA at telomeric DSBs in G1 human cells is not generated by conventional DSB or telomere resection machinery, nor does it in engage in resection-dependent recombinational repair, findings also consistent with the majority of telomeric ssDNA in G1 being 5' C-rich.

DISCUSSION

Telomere-specific DSBs have generally been regarded as irreparable, as DDRs generated globally by ionizing radiation or other genotoxic agents fail to resolve when they occur at or near telomeres, and cells become senescent (24, 25). While repair of targeted telomeric DSBs has been observed in cycling cell populations, as well as specifically in S-phase, there is a dearth of evidence for DDRs or repair activity at telomeric DSBs in G1 cells

(22, 23). To better understand human cellular responses to telomeric DSBs in G1, we investigated EN-T telomere-targeted DSBs, specifically in human BJ1hTERT (normal) and EJ-30 (cancer) cells.

Telomeric DSBs in G1 elicited an early DDR, as evidenced by γ-H2AX and MDC1 recruitment to telomere break sites. Notably however, 53BP1, a commonly used DDR marker, was recruited to telomeric DSBs in S/G2 – but *not* to those in G1 cells. Functionally, 53BP1 is most often associated with cNHEJ, where it restricts 5'-to-3' end-resection, but 53BP1 can also partially restrict resection during alt-NHEJ and HR repair (38, 43).

To gain mechanistic insight into this unexpected finding, we explored whether components of the telomere end-protection complex shelterin (12, 13) might be involved in thwarting 53BP1 recruitment to telomeric DSBs in G1 human cells. Telomere end-protection function was manipulated, without completely disrupting it, in an effort to alleviate inhibition of 53BP1 recruitment to telomeric DSBs while also avoiding dysfunctional telomere-induced foci (TIFs) (44). As near complete siRNA knockdown of telomere repeat factor 2 (TRF2) is necessary for a TIF response, we utilized an siRNA sequence that resulted in partial, sub-TIF-inducing depletion of TRF2, and combined it with EN-T or TRF1 transfection in BJ1 hTERT cells. While partial TRF2 knockdown did not result in a TIF response in untransfected cells, it also did not alleviate inhibition of 53BP1 recruitment to telomeric DSBs in G1 transfected cells. Depletion of TRF2 in EN-T transfected EJ-30 cells also did not affect telomere fragmentation, indicating that TRF2 does not impact telomeric DSB repair. The absence of 53BP1 at telomeric DSBs in G1 was also observed in EN-T-transfected human cells depleted of another potential candidate, DNA-PKcs, previously shown to play a role in mammalian telomere end protection (45), and proposed to act in concert with TRF2 in preventing both c-NHEJ and alt-NHEJ at functional telomeres (46).

Compaction of telomeric chromatin has been proposed as a unifying physical mechanism by which shelterin protects telomeres from repair (14, 47). Therefore, we tested

whether decompaction of genomic DNA could alleviate the repression of 53BP1 recruitment to telomeric DSBs in G1 human cells. Similar to partial TRF2 knockdown, treatment of EN-T transfected cells with a histone deacetylase inhibitor failed to result in recruitment of 53BP1 to G1 telomeric DSBs, suggesting that it may not be possible to relieve any potential influence of shelterin-mediated end-protection on inhibition of 53BP1 recruitment to telomeric DSBs in G1 without full deprotection of telomeres.

Consistent with the lack of 53BP1 recruitment to G1 telomeric DSBs, no evidence of cNHEJ cells was observed, as neither shRNA depletion of DNA-PKcs nor chemical inhibition of DNA-PKcs catalytic activity influenced the response to EN-T-inducted telomeric DSBs. Considering that both 53BP1 and cNHEJ impede DSB repair associated DNA resection, we hypothesized that telomeric DSBs in G1 human cells may be especially vulnerable to resection. Indeed, RPA coated ss telomeric DNA was detected following EN-T-induction of telomeric DSBs in G1, suggestive of extensive resection at break sites; the detection limit of FISH is on the order of 0.5 Kb (48). Importantly and consistent with rapid truncation events and overall telomere shortening, telomeric DSBs in G1 human cells facilitated formation and enrichment of 5’ C-rich ss telomeric DNA, an observation supported by minimal dependence on MRE11, EXO1, or Apollo exonucleases. Given the abundance of telomeric ss DNA at broken telomeres, a potential role for resection-dependent repair was also interrogated, however no evidence of RAD51 (HR/BIR), RAD52 (BIR/SSA), or BrdU incorporation was observed. Alt-NHEJ was also not a likely candidate for telomeric DSB repair in G1, since it utilizes only a few base pairs of homology (~20) (49, 50), and is hindered by RPA binding to ssDNA (51).

Although telomeric DSBs in G1 undergo extensive resection, they do not appear to be repaired in G1. One option may be that they reconstruct a 3’ G-rich ss overhang in order to form a protective t-loop and avoid cNHEJ-mediated telomere-telomere fusion (**Fig 7**). Interestingly, both 3’ G-rich and 5’ C-rich telomeric overhangs have been proposed to mediate t-loop

formation (31, 52). Therefore, resection may serve to stabilize broken telomeres during G1. This idea is supported by the fact that naturally shortened telomeres do not undergo fusion until nearly all telomeric repeats have been lost, suggesting that telomeres of nearly any length can be protected from repair activity (53). Furthermore, ss telomeric overhangs at functional telomeres have been implicated in protection from repair (54). To extend this line of reasoning, resected telomeric DSBs may simply persist into S-phase, where telomeres shortened by DSBs could be elongated via telomerase or recombination-based ALT mechanisms (**Fig 7**).

It also remains possible that some presently unappreciated pathway of repair operates at telomeric DSBs in G1 human cells. Potential candidates include RAD52-independent single-strand annealing (SSA), as SSA was recently shown to take place in RAD52$^{-/-}$ cells (55). Additionally, RNA-mediated DSB repair has recently been reported in human cells, a pathway that would be resection dependent and potentially not mediated by other conventional repair factors (56, 57). Our finding of 5' C-rich ss telomeric DNA at telomere-specific DSB break sites is particularly relevant in this regard, since 5' C-rich telomeric overhangs are previously reported outcomes of rapid truncation events that provide proposed markers of the recombination and replication dependent ALT pathway of telomere length maintenance (31, 58) We speculate that telomeric RNA or TERRA (59) may play a critical role in protecting telomeric DSB-induced 5' C-rich overhangs in G1, as TERRA is complementary in sequence, and present at elevated levels in ALT cells. Whether telomeric DSBs are indeed repaired in G1 by a novel alternative HR-based, replication *independent* pathway of repair, or they are preserved and processed by replication dependent mechanisms after progression into S/G2 phase, remains to be determined.

MATERIALS AND METHODS

Cell Culture and Transfections

U2OS cells, U2OS RAD52-YFP (obtained from Jiri Lucas, University of Copenhagen), and EJ-30 cells (obtained from Dr. John Murnane, UCSF) were cultured in Dulbecco's Modified Eagle Medium (DMEM, Hyclone) supplemented with 10% fetal bovine serum (FBS). BJ1 hTERT (ATCC), were cultured in Alpha-MEM (Hyclone) supplemented with 10% FBS. Transient transfections were carried out with Lipofectamine 3000 at 60-80% confluency in Opti-MEM (Gibco) for 20 minutes and replaced with normal media 8 hours later. Unless otherwise specified all experiments were carried out 48 hrs post transfection.

Laser Micro-Irradiation

Laser micro-irradiations were performed with a Zeiss LSM880 confocal microscope using a 405nm laser at 100% with settings of 50 iterations and a 15 us pixel dwell. Spatially defined stripes of damage were generated through the nuclei of cells followed by a recovery period of 30 min. Immunofluorescence and imaging of micro-irradiated cells was carried out as described below.

RNA interference

siRNA was initially delivered into cells using RNAiMAX in OptiMEM media according to manufacturer instructions, followed by replacement with normal media 5 hours later. 24 hours following initial siRNA delivery, cells were co-transfected with EN-T or TRF1 and appropriate siRNA in Lipofectamine 3000 according to manufacturer instructions, and then fixed or harvested 48hrs later. siRNA sequences were as follows: TRF2: 5'-GAGGAUGAACUGUUUCAAGdtdt-3' (anti-sense also included 3' dtdt), EXO1: 5'-UGCCUUUGCUAAUCCAAUCCCACGC-3'.

Inhibitors

BJ1hTERTs were treated with either a DNA-PKcs kinase inhibitor that prevents autophosphorylation (NU7026, Sigma) or MRE11 endonuclease activity inhibitor (PFM01, Thermofisher). NU7026 was used at a concentration of 10uM for 24 hours prior to harvesting cells as per previous (60). Alternatively, PFM01 was used at a concentration of 100uM for 8 hours preceding fixation. For chromatin relaxation, cells were treated with trichostatin A (TSA, Sigma) at the specified concentrations for 24 hrs prior to cell fixation.

Western Blotting

Cell pellets were washed in phosphate buffered saline (PBS), and then incubated in lysis buffer for 10 minutes. Lysis buffer consisted of Mammalian Protein Extraction Reagent (M-PER, ThermoFisher) with protease inhibitors (complete mini EDTA free, Sigma-Aldrich), and in cases when phosphorylated proteins were being detected, phosphatase inhibitors (PhosSTOP, Sigma-Alrdrich). Following isolation of protein, the Bradford assay was used to quantify protein (BioRad). 30ug of protein was loaded into precast SDS-PAGE gels (Mini-Protean TGX, 4-15%, BioRad) in Tris/Glycine/SDS buffer followed by electrophoretic separation for roughly 1.5 hours at 125V. After electrophoresis, proteins were transferred to a polyvinylidene fluoride (PVDF) membrane in Tris/Glycine buffer with 10-15% methanol for 16-20 hrs at 30V at 4^{o}C. An even protein transfer was verified by reversibly staining membranes with Poncaeu S solution (Sigma-Aldrich, 0.1% w/v in 1% acetic acid). Next, membranes were blocked in 5% non-fat dry milk (NFDM), or bovine serum albumin (BSA) in 1X Tris buffered saline with 0.1% Tween 20 (TBST) from 30 minutes to 1 hour with gentle shaking. Blocking solution was then replaced with fresh blocking solution containing the appropriate dilution of primary antibody and incubated from 2 hours to overnight with gentle shaking. Following primary antibody incubation, membranes were washed in 1X TBST for 4 washes of 10 minutes each with gentle shaking. Next, fresh blocking solution was added with the appropriate dilution of a horseradish peroxidase (HRP) labeled

secondary antibody and incubated from 2 to 4 hours followed by another series of 4 washes in 1X TBST. Following the final wash, membranes were rinsed in PBS. To visualize proteins, membranes were treated with SuperSignal™ West Pico Chemiluminescent Substrate according to the manufacturer instructions (ThermoFisher) and imaged on a ChemiDoc™ XRS+ imager with ImageLab™ software (BioRad).

Antibodies and Concentrations for Western Blotting

Primary antibodies for western blotting included Rabbit Anti-phospho serine2056 DNA-PKcs (Abcam ab1249181, 1:2000), Mouse Anti-DNA-PKcs (ThermoFisher MS-423-P, 1:10000), Mouse Anti-TRF2 (SantaCruz sc-271710, 1:500), Mouse Anti-phospho serine1981 ATM (Upstate 05-740, 1:1000), Rabbit Anti-phospho Thr68 CHK2 (Cell signaling 2661, 1:1000), Rabbit Anti-EXO1 (Proteintech 16352-1-AP, 1:500)

HRP labeled secondary antibodies included Donkey Anti-Rabbit (Jackson ImmunoResearch 711-035-152, 1:20000), and Rabbit Anti-Mouse (ThermoFisher 816720, 1:10000).

Immunofluorescence

Unless stated otherwise, cells were grown on chamber slides, rinsed twice in PBS, fixed in freshly prepared 4% paraformaldehyde (PFA) for 10 min at room temperature, and then permeabilized in 0.2% Triton X-100 in PBS for 4-10 minutes. Next, cells were blocked in 10% normal goat serum (NGS), or 5% BSA in 1xPBS for 40 minutes and then incubated with primary antibodies diluted in blocking solution for 1 hour at 37°C or overnight at 4°C. Following primary incubations cells were washed 3 times in 1xPBS at 42°C. After washes cells were incubated with fluorophore-conjugated goat secondary antibodies for 30 minutes at 37°C. Finally, cells were washed again as before and counterstained with Prolong Gold Antifade reagent with DAPI (Invitrogen).

BrdU Incorporation Assay

Cells were pulse-labeled with the thymidine analog BrdU (Bromodeoxyuridine / 5-bromo-2'-deoxyuridine; ThermoFisher) for 2 hours (50mM) and then fixed for 15 minutes in 4% PFA at room temperature. Next, cells were permeabilized for 20 min with 0.1% Triton x-100 in PBS, followed by DNA denaturation for 10 minutes on ice with 1N HCl and then 10 minutes at room temperature with 2N HCL. Cells were then washed with phosphate citric acid buffer pH 7.4 for 10 minutes at room temperature. Finally, cells were washed for 5 min in permeabilization solution. Blocking was then carried out for 30 min at 37C in 5% NGS with 0.1% Triton X-100 in PBS. Finally, antibody incubations, washing steps, and counterstaining were carried out as described in the immunofluorescence section.

Non-denaturing Immuno-FISH

Combined immunofluorescence and fluorescence in-situ hybridization (FISH) experiments were carried out on cells grown on chamber slides. Cells were initially fixed in 4% PFA for 5 minutes at room temperature. Next, cells were permeabilized for 4 minutes in 0.2% Triton X-100 in PBS. Following permeabilization, cells were blocked and immunostained as described in the immunofluorescence section. After the last washing step, cells were post-fixed in 4% PFA for 15 minutes at room temperature. Next, cells were dehydrated in an ethanol series (75%, 85%, 95%) for 2 minutes each and allowed to air dry. While slides were air drying, the hybridization solution was prepared by combining 36ul formamide, 12ul 0.05M Tris-HCL, 2.5ul 0.1M KCL, 0.6 ul 0.1M $MgCl_2$ and 0.5ul 0.5uM Peptide Nucleic Acid (PNA) telomere probe (TelC-Alexa488 or TelG-Cy3, Biosynthesis) in 20% acetic acid. Hybridization solution was then denatured at 85^{o}C for 10 min followed by cooling on ice. After cooling, 50ul of hybridization solution was added to each slide, then slides were coverslipped, and incubated at 37^{o}C in a humidified chamber for 6 hrs. Following hybridization, coverslips were removed and slides

washed twice in 50% formamide in 2X SSC (2.5 minutes 42°C), twice in 2X SSC (2.5 minutes 42°C) and twice in 2X SSC + 0.1% NP-40 (2.5 minutes 42°C). Following the final wash, cells were counterstained with Prolong Gold Antifade with DAPI.

Antibodies and Concentration for Immunofluorescence

Primary antibodies and concentrations included: Rabbit Anti-53BP1 (Bethyl A300-272A, 1:800), Rabbit Anti- γ-H2AX (Bethyl A300-081, 1:1000), Mouse Anti-Flag (Sigma M2 F1804, 1:2000-4000), Rabbit Anti-RPA70 (Cell signaling #2267, 1:50), Rabbit Anti-phospho S4/S8 RPA32 (Bethyl A300-245A 1:2000), Mouse Anti-gammaH2AX (Millipore 05-636, 1:1500), Rabbit Anti-Cyclin A (Santa Cruz SC-751, 1:500), Rabbit Anti-MDC1 (Bethyl A300-051A, 1:1000), Rabbit Anti-RAD51 (H-92 SC-8349, 1:800), Sheep Anti-RAD52 (kind gift from Jiri Lukas Lab, 1:100), Rat anti-BrdU (BioRad OBT0030, 1:200), Rabbit Anti-phospho S15 p53 (Abcam Ab18128-50, 1:500)

Secondary antibodies and concentrations included: Alexa-488 Goat anti-Mouse (ThermoFisher A11029, 1:750), Alexa-594 Goat anti-Mouse (ThermoFisher A11005, 1:750), Alexa-647 Goat anti-Mouse (ThermoFisher A21235, 1:350), Alexa-488 Donkey anti-Mouse (ThermoFisher 21202, 1:750), Alexa-488 Goat anti-Rabbit (ThermoFisher A11008, 1:750), Alexa-594 Goat anti-Rabbit (ThermoFisher A11012, 1:750), Alexa-555 Goat anti-Rat (ThermoFisher A21434, 1:750), Alexa-647 Donkey anti-Sheep (ThermoFisher A21448, 1:350), Alexa-488 Donkey anti-Mouse (ThermoFisher A21202 1:750)

Fluorescence Microscopy and Image Analysis

Images were acquired using a Zeiss Axio Imager.Z2 epi-fluorescent microscope using a 63X/1.4 N.A. objective (Plan-APOCHROMAT, Zeiss). For the majority of targets, images were blindly and subjectively thresholded and segmented followed by determination of foci overlap (50% overlap scored as positive) in Metamorph 7.7 (Molecular Devices). For RAD52-YFP, RPA

and phospho-RPA foci analysis, cells tended to have very few or an abundance of foci and scoring was therefore done on the basis of whether a cell had >4 foci overlapping Flag.

Analysis of the laser microirradiation experiment involved first thresholding TRF2 foci using a fixed value for all images. Next, these thresholded foci were converted to regions in Metamorph and these regions transferred to γ-H2AX or 53BP1 images. Next, the average intensity within the transferred regions was compared to that within pseudo-random regions of comparable dimensions generated by rotating TRF2 images by 90°.

For BrdU foci analysis in BJ1 hTERTs, untransfected S-phase cells were excluded from analysis (identified by very bright pan nuclear staining).

For DAPI-intensity based cell cycle analysis, DAPI intensity was collected alongside foci by subjective thresholding and segmentation in Metamorph followed by histogram generation. Foci counts were sorted based on whether the nuclear intensity fell into the clear G1 peak or the S/G2 tail. The border region between cell cycle phases of 4 DAPI intensity bins was excluded from analysis to be sure of an accurate classification of cells.

Telomere Restriction Fragment (TRF) Southern Blots

The TRF assay was performed using the TeloTAGGG™ southern blotting kit (Roche) according to the manufacturer instructions with some modifications, including a longer probe hybridization time (6hrs), as well as a longer incubation time with Anti-DIG antibody (1hr). 2ug of sample DNA were loaded per lane and blots were imaged on a ChemiDoc™ XRS+ imager with ImageLab™ software (BioRad). Quantitation of mean TRF length was performed using TeloTool software according to the manufacturer's protocol.

Plasmids

TRAS1-EN-TRF1 and TRF1 plasmids, both driven by a CMV promoter and possessing a C-terminal Flag tag for visualization, were constructed from a CMV-driven TRAS1-EN-TRF1 plasmid obtained from Dr. Haruhiko Fujiwara (University of Tokyo).

Replication, Statistics

EN-T validation experiments in U20S cells were done in duplicate (50 cells per replicate). Experiments in BJ1 hTERT cells involved 3 independent experiments for each condition with at least 30 cells per replicate for imaging experiments. The exception to this was micro-irradiation experiments, which were done in duplicate with 15 cells per replicate. Experiments in EJ-30 cells were also in triplicate; however, the number of cells imaged totaled at least 300 per condition to allow for DAPI intensity histogram generation.

Error bars on bar graphs represent standard deviations, and p-values were computed when experiments were done in triplicate, and are provided in the text when less than 0.05 (significance threshold). When two groups were being compared p-values were generated via students T-tests, alternatively, when three or more groups were being compared an ANOVA with a Tukey's post hoc test was used. ANOVAs were either one way or two way depending on the number of categorical independent variables.

CONFLICT OF INTEREST

The authors declare that there are no conflicts of interest.

ACKNOWLEDGEMENTS

The authors sincerely thank Dr. Haruhiko Fujiwara for generously supplying the TRAS1-EN-TRF1 and TRF1 plasmids, and Dr. Jiri Lucas for U2OS cell lines. We also gratefully acknowledge funding from NASA (NNX14AB02G).

REFERENCES

1. Meyne J, Ratliff RL, Moyzis RK. Conservation of the human telomere sequence (TTAGGG)n among vertebrates. Proc Natl Acad Sci USA. 1989;86(18):7049-53.

2. Makarov VL, Hirose Y, Langmore JP. Long G tails at both ends of human chromosomes suggest a C strand degradation mechanism for telomere shortening. Cell. 1997;88(5):657-66.

3. Greider CW, Blackburn EH. Identification of a specific telomere terminal transferase activity in Tetrahymena extracts. Cell. 1985;43(2 Pt 1):405-13.

4. Kim NW, Piatyszek MA, Prowse KR, Harley CB, West MD, Ho PL, et al. Specific association of human telomerase activity with immortal cells and cancer. Science. 1994;266(5193):2011-5.

5. Batista LFZ. Telomere biology in stem cells and reprogramming. Prog Mol Biol Transl Sci. 2014;125:67-88.

6. Bryan TM, Englezou A, Dalla-Pozza L, Dunham MA, Reddel RR. Evidence for an alternative mechanism for maintaining telomere length in human tumors and tumor-derived cell lines. Nat Med. 1997;3(11):1271-4.

7. Henson JD, Cao Y, Huschtscha LI, Chang AC, Au AYM, Pickett HA, et al. DNA C-circles are specific and quantifiable markers of alternative-lengthening-of-telomeres activity. Nat Biotechnol. 2009;27(12):1181-5.

8. Cesare AJ, Reddel RR. Alternative lengthening of telomeres: models, mechanisms and implications. Nat Rev Genet. 2010;11(5):319-30.

9. Bailey SM, Brenneman MA, Goodwin EH. Frequent recombination in telomeric DNA may extend the proliferative life of telomerase-negative cells. Nucleic Acids Res. 2004;32(12):3743-51.

10. Murnane JP, Sabatier L, Marder BA, Morgan WF. Telomere dynamics in an immortal human cell line. EMBO J. 1994;13(20):4953-62.

11. Griffith JD, Comeau L, Rosenfield S, Stansel RM, Bianchi A, Moss H, et al. Mammalian telomeres end in a large duplex loop. Cell. 1999;97(4):503-14.

12. de Lange T. Shelterin: the protein complex that shapes and safeguards human telomeres. Genes Dev. 2005;19(18):2100-10.

13. de Lange T. How Shelterin Solves the Telomere End-Protection Problem. Cold Spring Harbor Symposia on Quantitative Biology. 2010;75(0):167-77.

14. Baker AM, Fu Q, Hayward W, Victoria S, Pedroso IM, Lindsay SM, et al. The telomere binding protein TRF2 induces chromatin compaction. PLOS ONE. 2011;6(4):e19124.

15. Sfeir A, de Lange T. Removal of shelterin reveals the telomere end-protection problem. Science. 2012;336(6081):593-7.

16. de Lange T. A loopy view of telomere evolution. Front Genet. 2015;6:321.

17. van Steensel B, Smogorzewska A, de Lange T. TRF2 Protects Human Telomeres from End-to-End Fusions. Cell. 1998;92(3):401-13.

18. Bae NS, Baumann P. A RAP1/TRF2 complex inhibits nonhomologous end-joining at human telomeric DNA ends. Mol Cell. 2007;26(3):323-34.

19. Kibe T, Osawa GA, Keegan CE, de Lange T. Telomere protection by TPP1 is mediated by POT1a and POT1b. Mol Cell Biol. 2010;30(4):1059-66.

20. Anzai T, Takahashi H, Fujiwara H. Sequence-specific recognition and cleavage of telomeric repeat (TTAGG)(n) by endonuclease of non-long terminal repeat retrotransposon TRAS1. Mol Cell Biol. 2001;21(1):100-8.

21. Yoshitake K, Aoyagi H, Fujiwara H. Creation of a novel telomere-cutting endonuclease based on the EN domain of telomere-specific non-long terminal repeat retrotransposon, TRAS1. Mob DNA. 2010;1(1):13.

22. Mao P, Liu J, Zhang Z, Zhang H, Liu H, Gao S, et al. Homologous recombination-dependent repair of telomeric DSBs in proliferating human cells. Nat Commun. 2016;7:12154.

23. Doksani Y, de Lange T. Telomere-Internal Double-Strand Breaks Are Repaired by Homologous Recombination and PARP1/Lig3-Dependent End-Joining. Cell Rep. 2016;17(6):1646-56.

24. Hewitt G, Jurk D, Marques FDM, Correia-Melo C, Hardy T, Gackowska A, et al. Telomeres are favoured targets of a persistent DNA damage response in ageing and stress-induced senescence. Nat Commun. 2012;3:708.

25. Fumagalli M, Rossiello F, Clerici M, Barozzi S, Cittaro D, Kaplunov JM, et al. Telomeric DNA damage is irreparable and causes persistent DNA-damage-response activation. Nat Cell Biol. 2012;14(4):355-65.

26. Lieber MR. The Mechanism of Double-Strand DNA Break Repair by the Nonhomologous DNA End-Joining Pathway. Annual Review of Biochemistry. 2010;79(1):181-211.

27. Chapman JR, Taylor MRG, Boulton SJ. Playing the end game: DNA double-strand break repair pathway choice. Mol Cell. 2012;47(4):497-510.

28. Chang HHY, Pannunzio NR, Adachi N, Lieber MR. Non-homologous DNA end joining and alternative pathways to double-strand break repair. Nat Rev Mol Cell Biol. 2017;18(8):495-506.

29. Maréchal A, Zou L. RPA-coated single-stranded DNA as a platform for post-translational modifications in the DNA damage response. Cell Research. 2015;25(1):9-23.

30. Lam YC, Akhter S, Gu P, Ye J, Poulet A, Giraud-Panis M-J, et al. SNMIB/Apollo protects leading-strand telomeres against NHEJ-mediated repair. EMBO J. 2010;29(13):2230-41.

31. Oganesian L, Karlseder J. Mammalian 5' C-rich telomeric overhangs are a mark of recombination-dependent telomere maintenance. Mol Cell. 2011;42(2):224-36.

32. Zschenker O, Kulkarni A, Miller D, Reynolds GE, Granger-Locatelli M, Pottier G, et al. Increased sensitivity of subtelomeric regions to DNA double-strand breaks in a human cancer cell line. DNA Repair (Amst). 2009;8(8):886-900.

33. Miller D, Reynolds GE, Mejia R, Stark JM, Murnane JP. Subtelomeric regions in mammalian cells are deficient in DNA double-strand break repair. DNA Repair (Amst). 2011;10(5):536-44.

34. Muraki K, Han L, Miller D, Murnane JP. The role of ATM in the deficiency in nonhomologous end-joining near telomeres in a human cancer cell line. PLoS Genet. 2013;9(3):e1003386.

35. Cho NW, Dilley RL, Lampson MA, Greenberg RA. Interchromosomal homology searches drive directional ALT telomere movement and synapsis. Cell. 2014;159(1):108-21.

36. Dilley RL, Verma P, Cho NW, Winters HD, Wondisford AR, Greenberg RA. Break-induced telomere synthesis underlies alternative telomere maintenance. Nature. 2016;539(7627):54-8.

37. Stewart GS, Wang B, Bignell CR, Taylor AMR, Elledge SJ. MDC1 is a mediator of the mammalian DNA damage checkpoint. Nature. 2003;421(6926):961-6.

38. Xiong X, Du Z, Wang Y, Feng Z, Fan P, Yan C, et al. 53BP1 promotes microhomology-mediated end-joining in G1-phase cells. Nucleic Acids Res. 2015;43(3):1659-70.

39. Dimitrova N, Chen Y-CM, Spector DL, de Lange T. 53BP1 promotes non-homologous end joining of telomeres by increasing chromatin mobility. Nature. 2008;456(7221):524-8.

40. Zimmermann M, Lottersberger F, Buonomo SB, Sfeir A, de Lange T. 53BP1 regulates DSB repair using Rif1 to control 5' end resection. Science. 2013;339(6120):700-4.

41. Wu P, van Overbeek M, Rooney S, de Lange T. Apollo contributes to G overhang maintenance and protects leading-end telomeres. Mol Cell. 2010;39(4):606-17.

42. Wu P, Takai H, de Lange T. Telomeric 3' overhangs derive from resection by Exo1 and Apollo and fill-in by POT1b-associated CST. Cell. 2012;150(1):39-52.

43. Ochs F, Somyajit K, Altmeyer M, Rask M-B, Lukas J, Lukas C. 53BP1 fosters fidelity of homology-directed DNA repair. Nat Struct Mol Biol. 2016;23(8):714-21.

44. Cesare AJ, Hayashi MT, Crabbe L, Karlseder J. The telomere deprotection response is functionally distinct from the genomic DNA damage response. Mol Cell. 2013;51(2):141-55.

45. Bailey SM, Meyne J, Chen DJ, Kurimasa A, Li GC, Lehnert BE, et al. DNA double-strand break repair proteins are required to cap the ends of mammalian chromosomes. Proc Natl Acad Sci USA. 1999;96(26):14899-904.

46. Bombarde O, Boby C, Gomez D, Frit P, Giraud-Panis M-J, Gilson E, et al. TRF2/RAP1 and DNA-PK mediate a double protection against joining at telomeric ends. EMBO J. 2010;29(9):1573-84.

47. Bandaria JN, Qin P, Berk V, Chu S, Yildiz A. Shelterin Protects Chromosome Ends by Compacting Telomeric Chromatin. Cell. 2016;164(4):735-46.

48. Ramakrishnan S, Sulochana KN. Manual of Medical Laboratory Techniques: Jaypee Brothers Medical Publishers Pvt. Ltd.; 2012 2012/12/15/. 453 p.

49. Truong LN, Li Y, Shi LZ, Hwang PY-H, He J, Wang H, et al. Microhomology-mediated End Joining and Homologous Recombination share the initial end resection step to repair DNA double-strand breaks in mammalian cells. Proc Natl Acad Sci USA. 2013;110(19):7720-5.

50. Symington LS, Gautier J. Double-Strand Break End Resection and Repair Pathway Choice. Annual Review of Genetics. 2011;45(1):247-71.

51. Deng SK, Gibb B, de Almeida MJ, Greene EC, Symington LS. RPA antagonizes microhomology-mediated repair of DNA double-strand breaks. Nat Struct Mol Biol. 2014;21(4):405-12.

52. Verdun RE, Karlseder J. The DNA damage machinery and homologous recombination pathway act consecutively to protect human telomeres. Cell. 2006;127(4):709-20.

53. Capper R, Britt-Compton B, Tankimanova M, Rowson J, Letsolo B, Man S, et al. The nature of telomere fusion and a definition of the critical telomere length in human cells. Genes Dev. 2007;21(19):2495-508.

54. Gong Y, de Lange T. A Shld1-controlled POT1a provides support for repression of ATR signaling at telomeres through RPA exclusion. Mol Cell. 2010;40(3):377-87.

55. Kan Y, Batada NN, Hendrickson EA. Human somatic cells deficient for RAD52 are impaired for viral integration and compromised for most aspects of homology-directed repair. DNA Repair (Amst). 2017;55:64-75.

56. Meers C, Keskin H, Storici F. DNA repair by RNA: Templated, or not templated, that is the question. DNA Repair (Amst). 2016;44:17-21.

57. Mazina OM, Keskin H, Hanamshet K, Storici F, Mazin AV. Rad52 Inverse Strand Exchange Drives RNA-Templated DNA Double-Strand Break Repair. Mol Cell. 2017;67(1):19-29.e3.

58. Oganesian L, Karlseder J. 5' C-rich telomeric overhangs are an outcome of rapid telomere truncation events. DNA Repair (Amst). 2013;12(3):238-45.

59. Azzalin CM, Reichenbach P, Khoriauli L, Giulotto E, Lingner J. Telomeric repeat containing RNA and RNA surveillance factors at mammalian chromosome ends. Science. 2007;318(5851):798-801.

60. Le PN, Maranon DG, Altina NH, Battaglia CLR, Bailey SM. TERRA, hnRNP A1, and DNA-PKcs Interactions at Human Telomeres. Front Oncol. 2013;3:91.

Figure 1

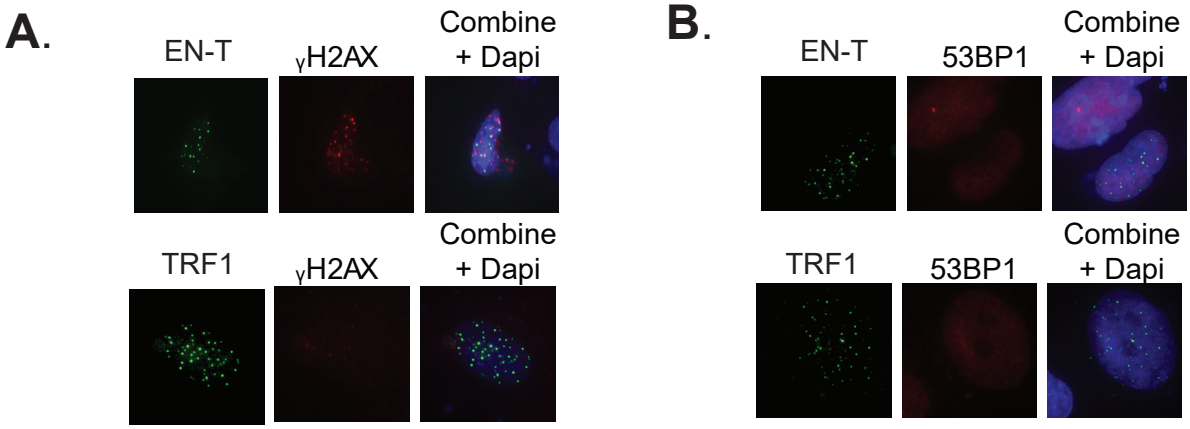

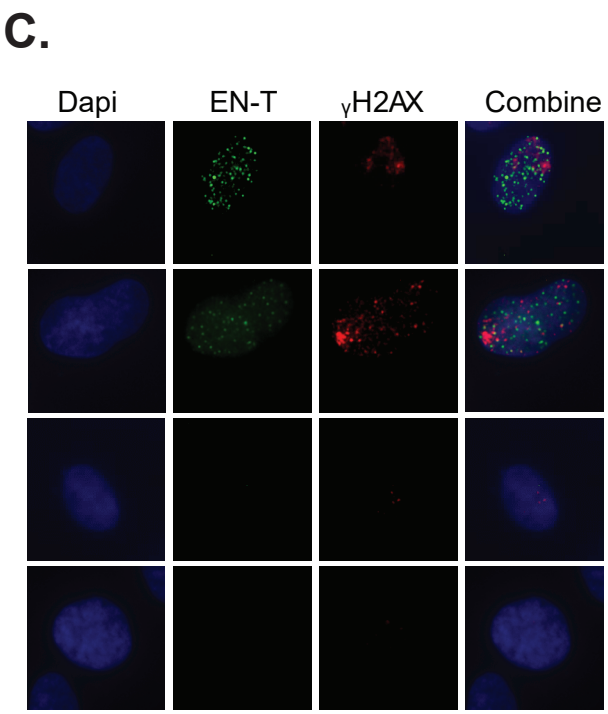

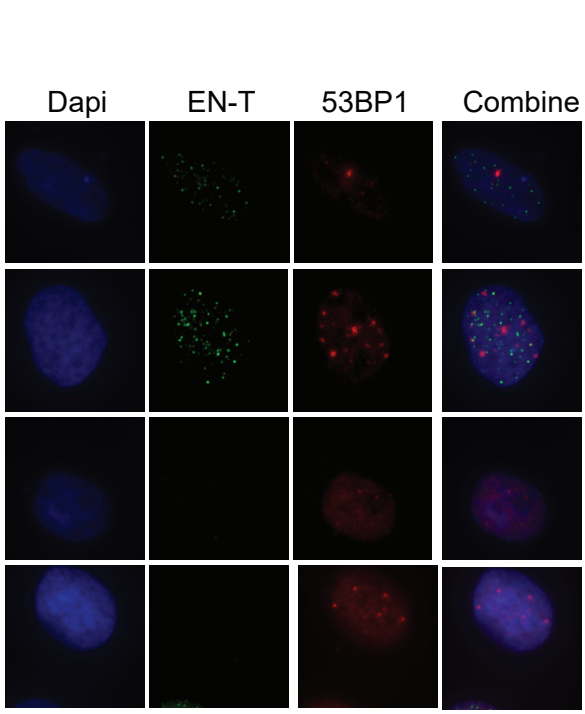

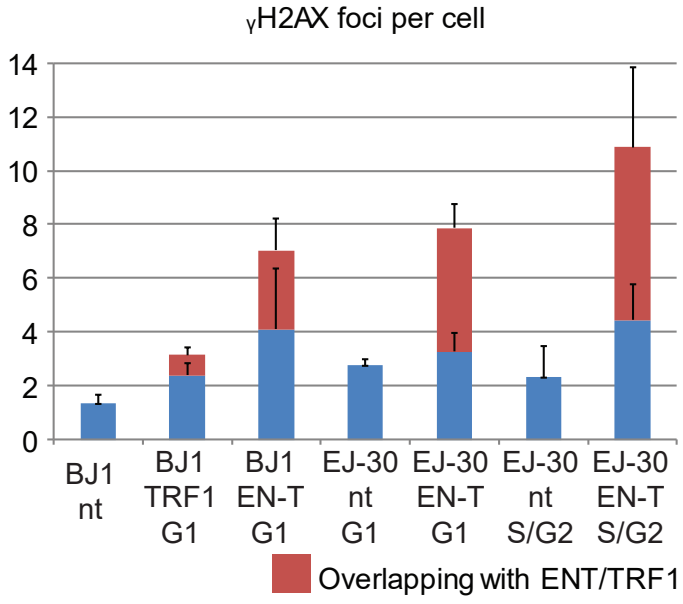

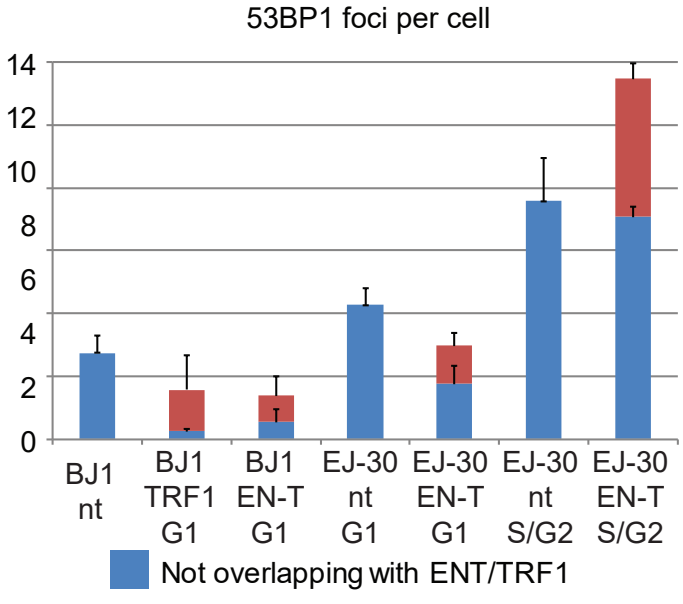

Figure 2

A.

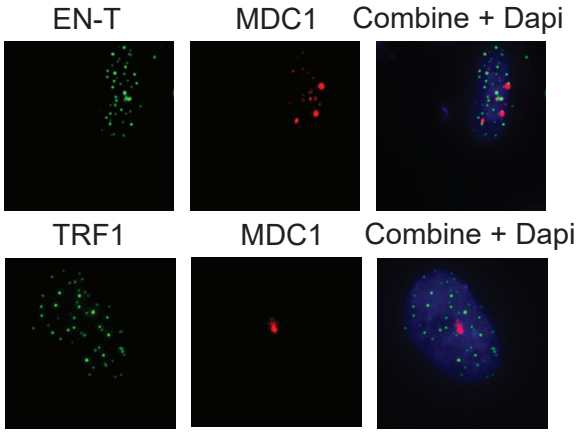

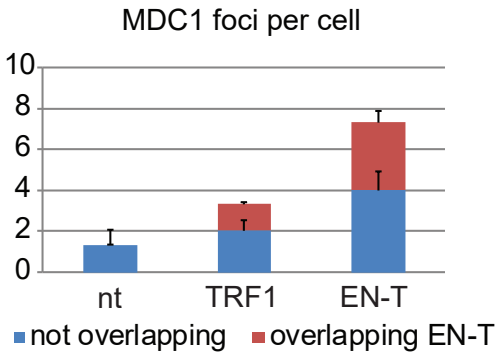

B.

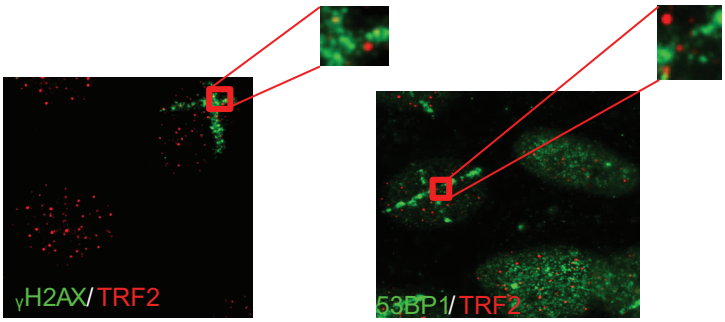

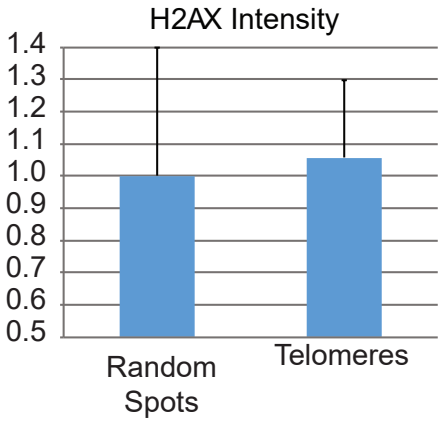

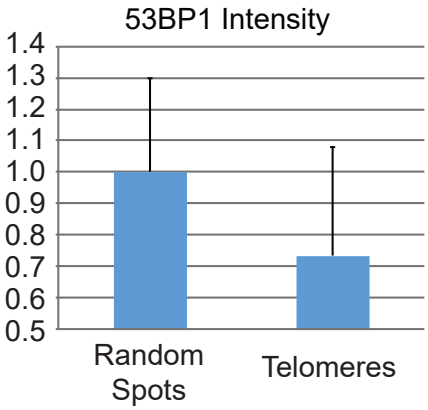

Figure 3

A.

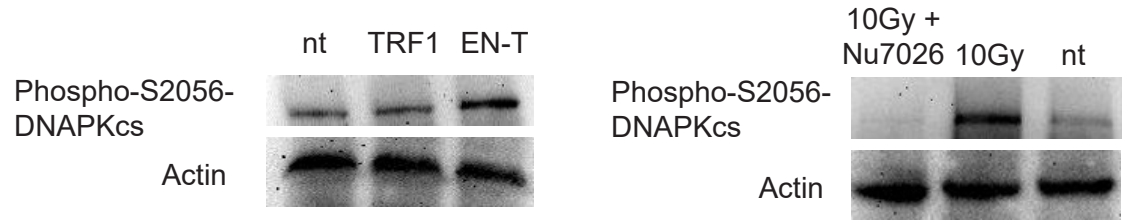

B.

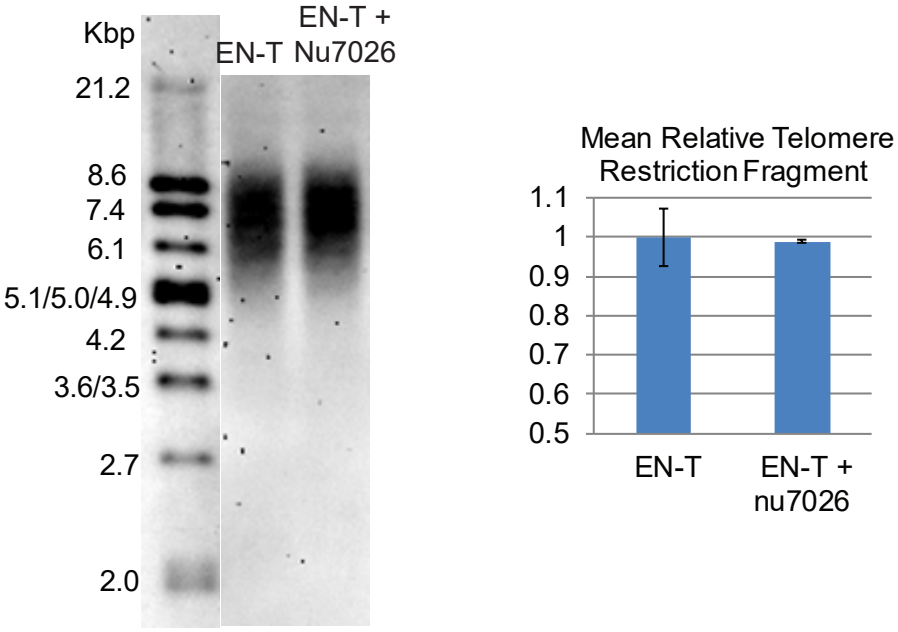

Figure 4

A.

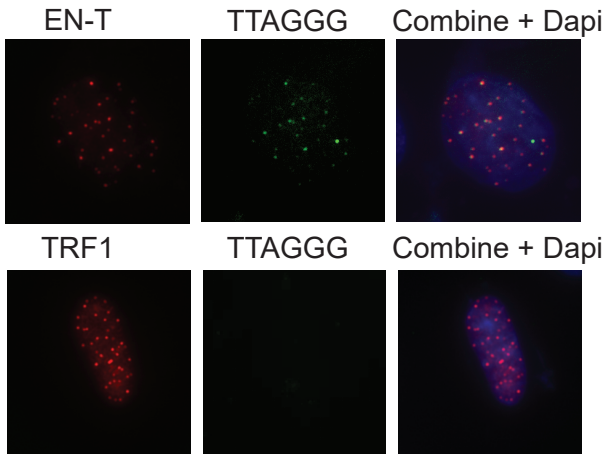

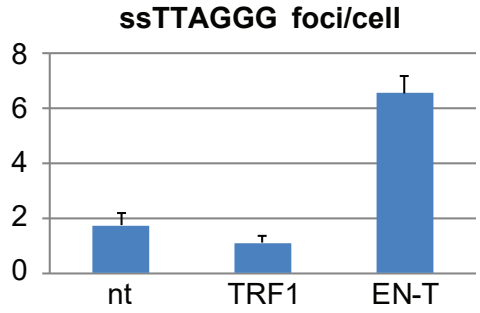

B.

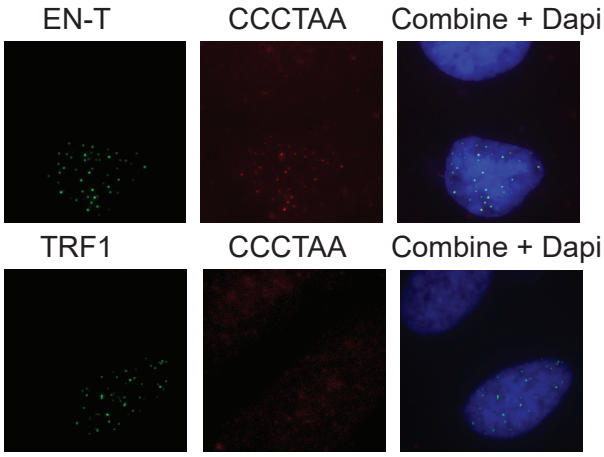

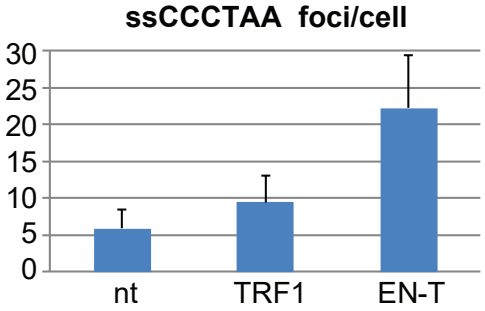

Figure 5

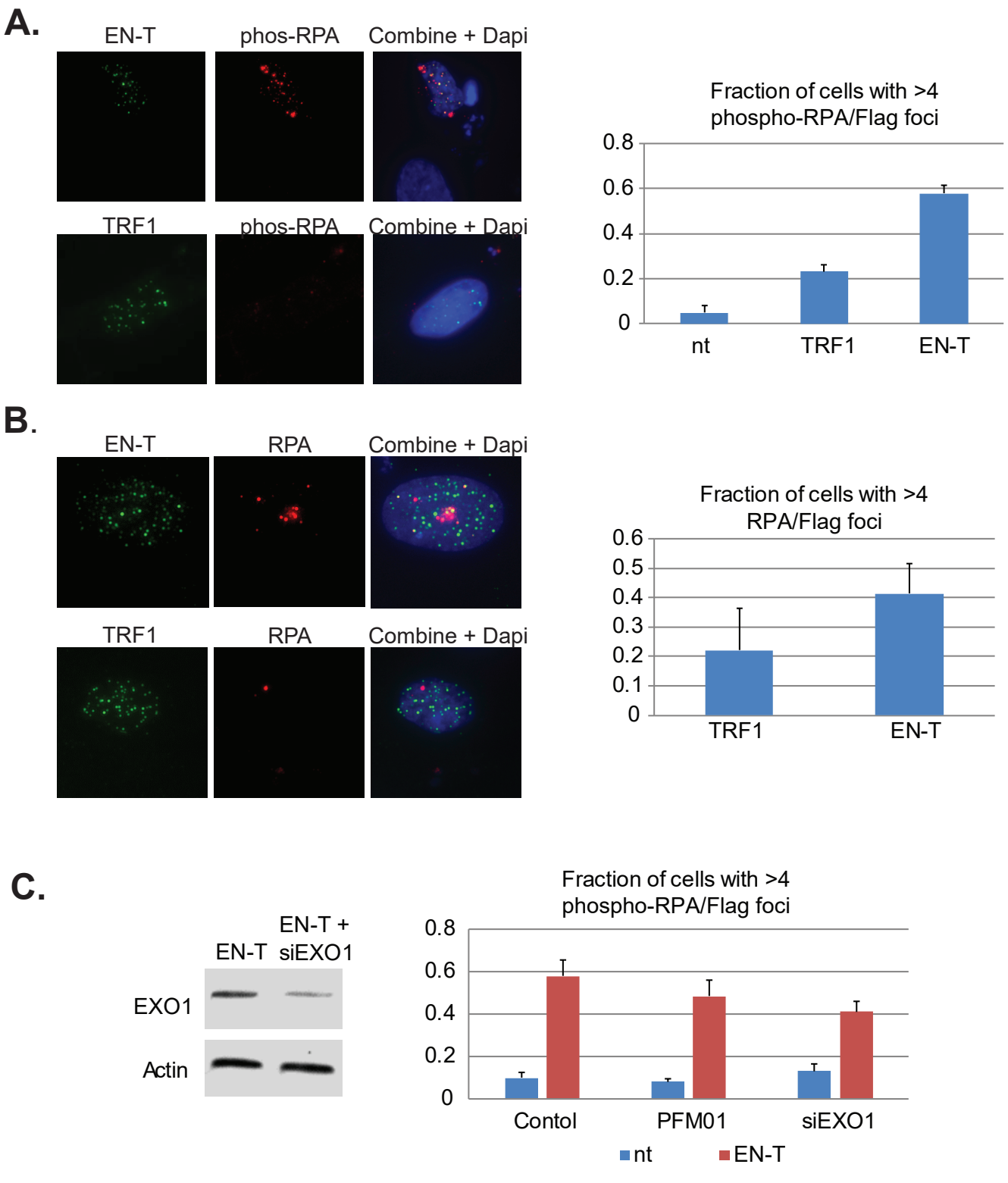

Figure 6

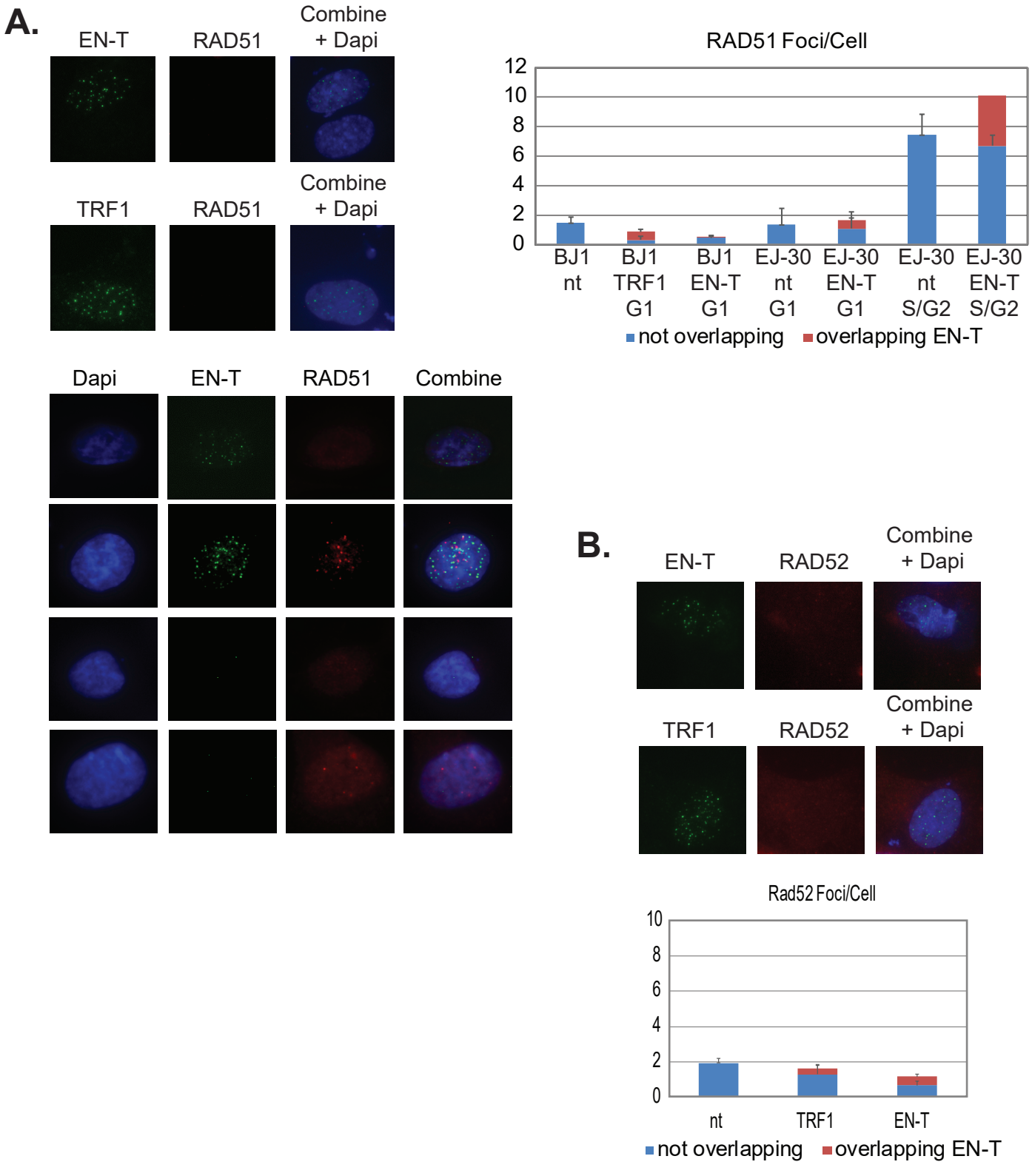

Figure 7

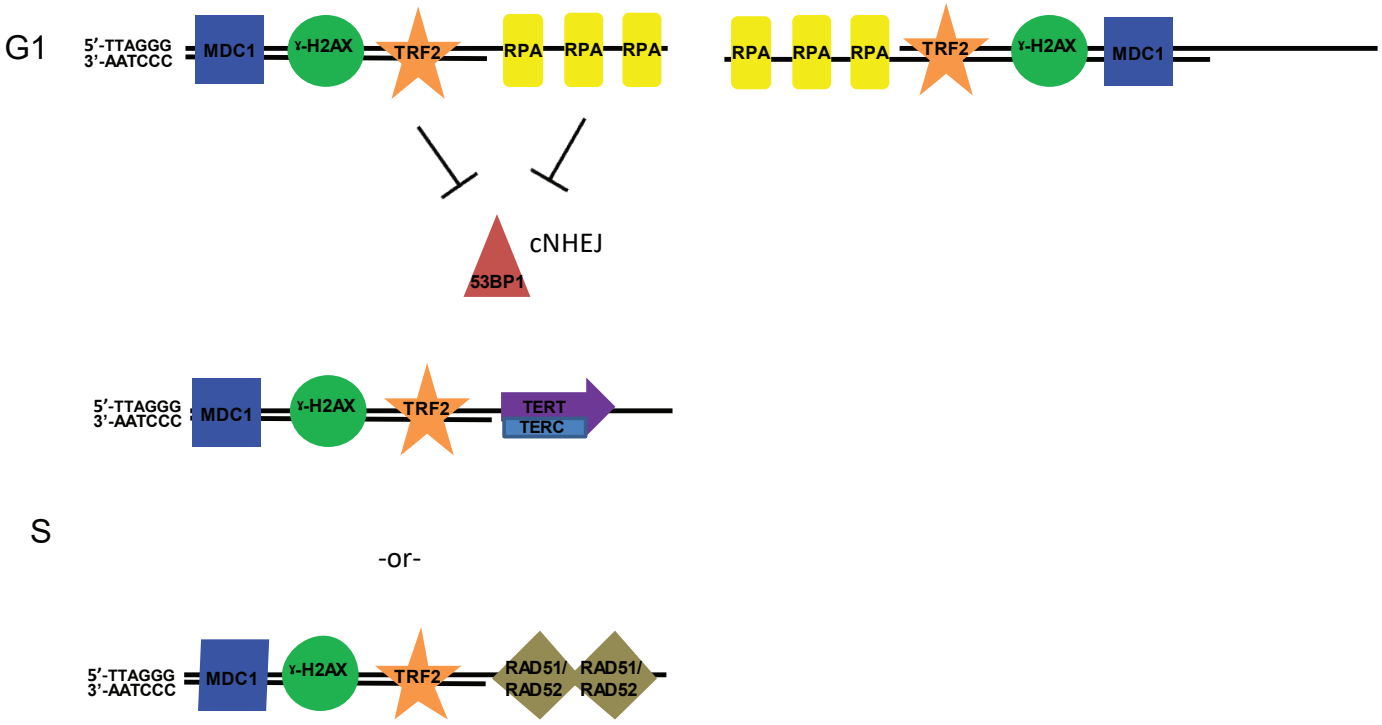

Supplemental Figure 1

A.

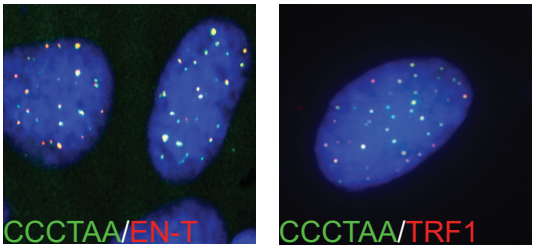

B.

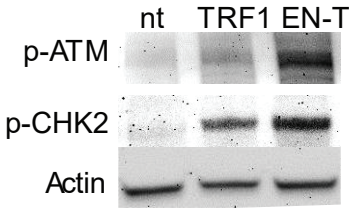

C.

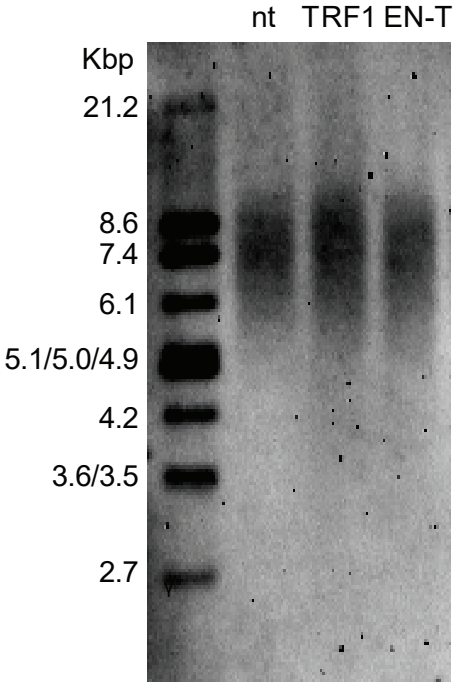

D.

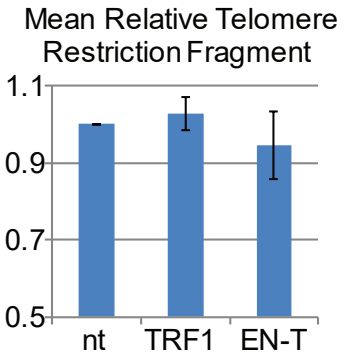

Supplemental Figure 2

A.

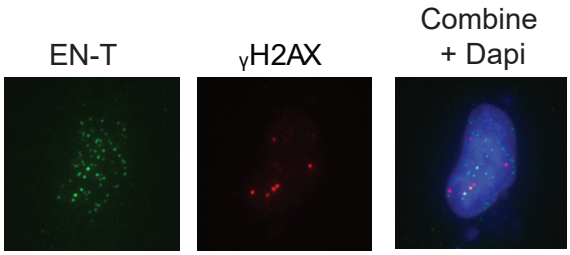

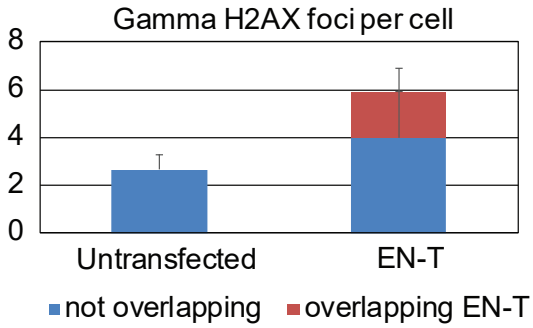

B.

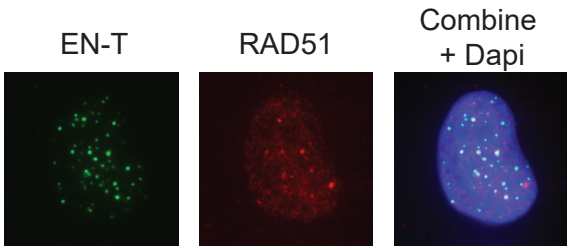

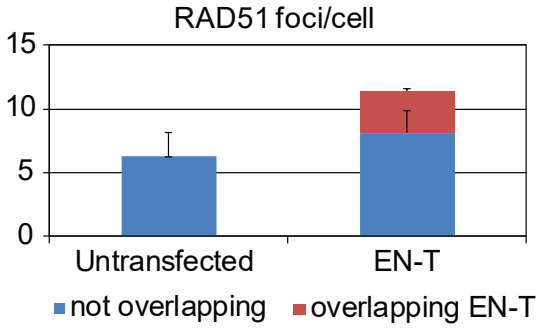

C.

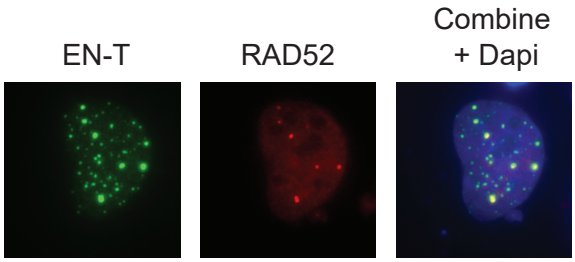

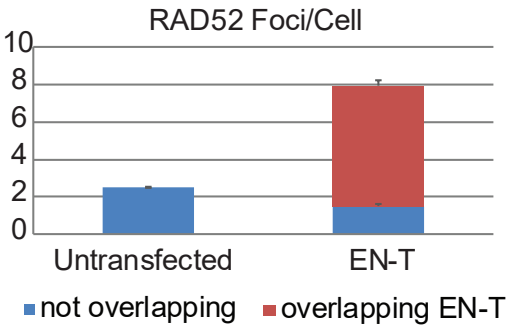

Supplemental Figure 3

A.

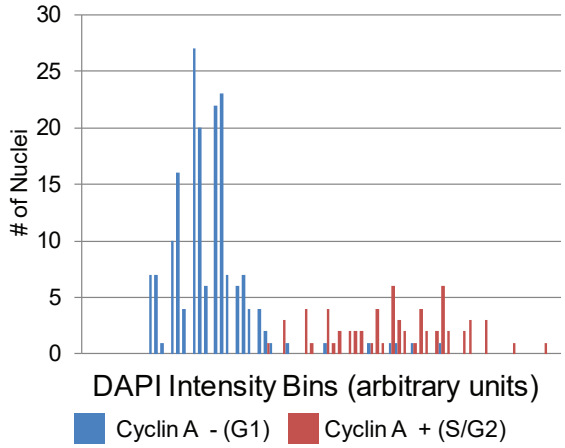

B.

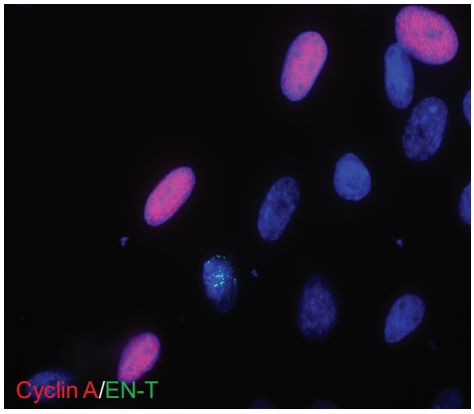

C.

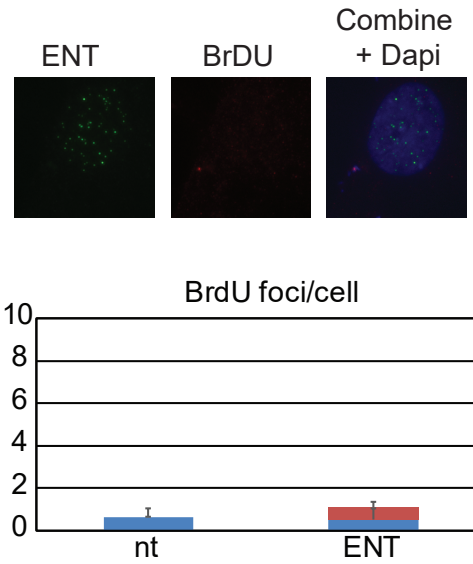

Supplemental Figure 4

A.

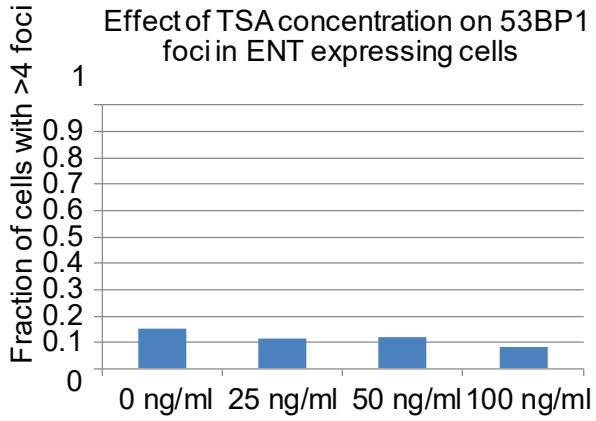

B.

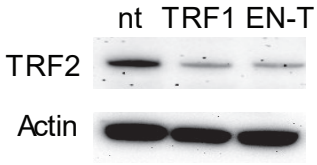

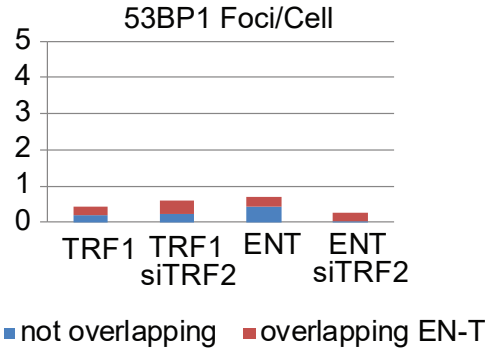

C.

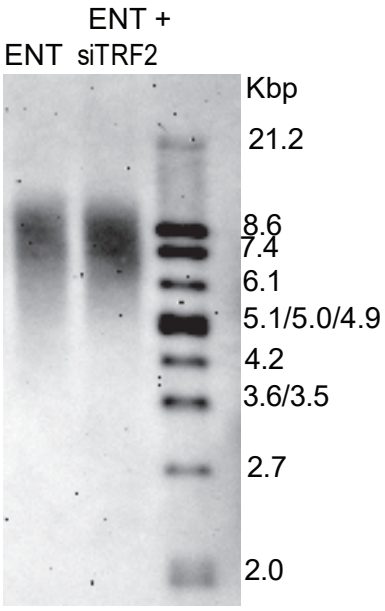

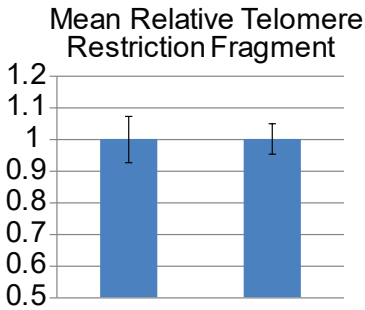

D.

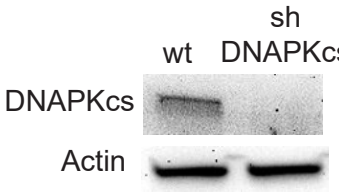

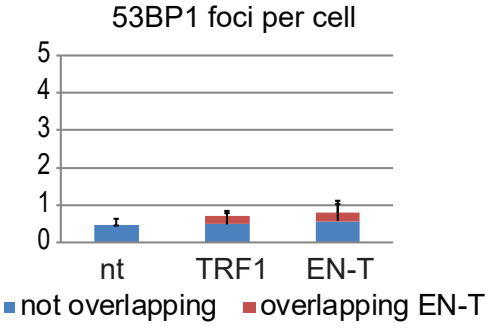

Supplemental Figure 5

A.

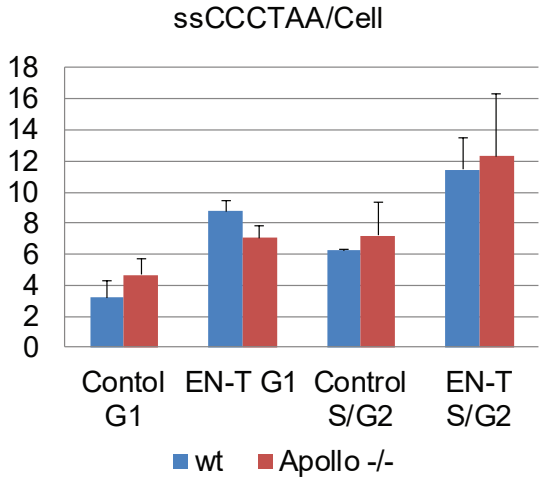

B.

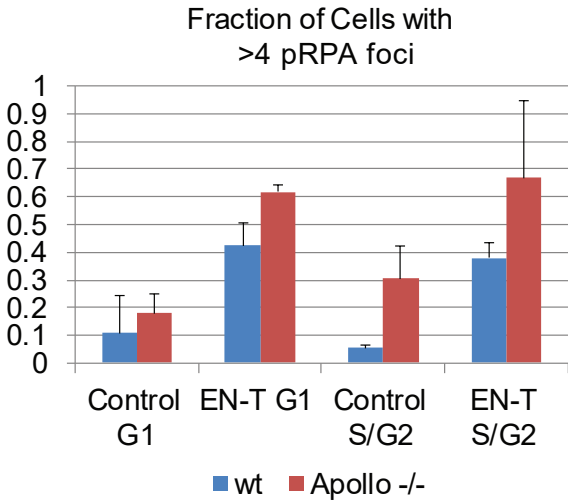

Figure 1:

Telomere-specific DSBs in G1 do not attract 53BP1 to break sites. **A.** γ-H2AX foci co-localized with broken telomeres following transfection with EN-T in BJ1 hTERT G1 cells (p=0.012). **B.** However, 53BP1 foci did not co-localize with broken telomeres in BJ1 hTERT G1 cells. **C, D**. EJ-30 cells displayed similar G1 DNA damage response activation as BJ1 hTERT cells. While telomere DSB induction by EN-T stimulated γ-H2AX foci at telomeres in both G1 and S/G2 cells (p = 0.0009 and 0.022 respectively), 53BP1 foci were only induced at telomeres in S/G2 cells (p = 0.012).

Figure 2:

DNA damage response at broken telomeres in G1. **A.** Transfection with EN-T also resulted in an increased number of MDC1 foci in BJ1 hTERT G1 cells (compared to non-transfected and TRF1 control cells), which often overlapped with ENT-flag (p = 0.0007). **B**. The intensity of γ-H2AX within microirradiation stripes was similar at telomeres and random spots in non-transfected BJ1 hTERT cells, while the intensity of 53BP1 within microirradiation stripes was decreased at telomeres relative to random spots (p=0.099).

Figure 3:

Minimal role of cNHEJ at telomeric DSBs in G1. B. **A.** Autophosphorylation of DNA-PKcs at S2056 was induced following EN-T transfection of EJ-30 cells. DNA-PKcs autophosphorylation following exposure to 10Gy ionizing radiation (gamma-rays) was prevented by the specific kinase inhibitor NU7026. **B.** Treatment with NU7026 did not influence mean TRF length in EJ-30 cells transfected with EN-T.

Figure 4:

Extensive resection at telomeric DSBs in G1 enriches 5' C-rich ssDNA. **A.** Transfection of BJ1hTERT cells with EN-T promoted modest production of ssDNA at the G-rich telomere (5'-

TTAGGG-3') (p = 0.0002). **B.** Consistent with bidirectional resection at telomeric DSBs, ssDNA was also associated with the C-rich telomere (5'-CCCTAA-3') (p = 0.045), which was present at a much higher frequency.

Figure 5:

Extent of RPA-coated ssDNA at telomeric DSBs in G1 BJ1 hTERT cells is not significantly influenced by MRE11 or EXO1 nuclease activity. **A.** EN-T expression in BJ1 hTERT cells induced both phospo-RPA32 and **B.** RPA70 foci that overlapped with ENT-flag (phospho RPA-32 p = 0.0000046, RPA70 p = 0.27.). **C**. Phospho-RPA32 induction following EN-T transfection was not significantly reduced by either inhibition of MRE11 endonuclease activity (PFM01) or siRNA knockdown of EXO1 (p = 0.24, 0.057, respectively).

Figure 6:

Minimal role of HR at telomeric DSBs in G1. **A.** Transfection of G1 BJ1 hTERT or EJ-30 cells with EN-T did not induce RAD51 foci. RAD51 foci were slightly increased in S/G2 EJ-30 cells following expression of EN-T, consistent with HR activity. **B**. Transfection of G1 BJ1 hTERT cells with EN-T also did not induce RAD52 foci.

Figure 7:

Speculative model. Telomere-specific DSBs in G1 human cells initiate a DDR (MDC1 and γ-H2AX), but do not recruit 53BP1, nor do they undergo cNHEJ. Extensive resection does occur, producing primarily 5' C-rich ss telomeric overhangs coated with RPA, which do not participate in HR/BIR/SSA. We speculate that RPA coated sstelomeric DNA functions to prevent 53BP1 recruitment, thereby hampering cNHEJ. In this scenario, telomeric DSBs in G1 are prevented from engaging in repair activities, being resected potentially to enable end-protection until they can be repaired/extended during S-phase by telomerase or recombinational repair.

Supplemental Figure 1:

Characterization of telomere-specific cutting endonuclease TRAS-ENT (ENT). **A.** Overexpressed EN-T or TRF1 co-localized with telomere repeats in U20S, EJ-30, and BJ1 hTERT cells (shown). **B.** Expression of ENT in EJ-30 cells activated DDR signaling, evidenced by P-S1981-ATM and P-Thr68-CHK2. **C.** Expression of ENT in EJ-30 cells resulted in fragmentation of telomeric DNA on southern blot of telomeric restriction fragments (TRF); **D.** quantification of non-transfected (nt), TRF1 control, and ENT transfected cells**.**

Supplemental Figure 2:

Additional characterization of EN-T system. **A.** Transfection of cycling U20S (ALT) cells with EN-T triggered a telomeric DDR in terms of γ-H2AX foci, which frequently overlapped with ENT-flag (red bar). **B, C.** Induced telomeric DSBs in cycling U20S cells also stimulated recruitment of RAD51 and RAD52, mediators of HR and BIR respectively, both of which frequently overlapped with ENT-flag.

Supplemental Figure 3:

DAPI intensity histograms to identify cells in G1. **A.** DAPI intensity histograms were generated from 63X images of approximately 300 cells per experiment. Exclusion of Cyclin A from the low DAPI intensity peak region of the histogram (blue bars) verified that these cells were in G1 phase of the cell cycle; data shown represent merged histograms from 3 replicates totaling 300 EJ-30 cells. **B.** DAPI intensity histograms were not necessary for identification of G1 BJ1 hTERT cells, as ENT and TRF1 transfected cells were almost exclusively negative for Cyclin A, consistent with the vast majority of transfected BJ1 hTERT cells being in G1 phase 48 hr post transfection. Image illustrates that while the population of cells contains many cyclin A positive cells (red), the relatively few transfected cells (green

foci; EN-T) were always cyclin A negative (in G1). **C**. Repair associated DNA synthesis (BrdU incorporation) was also not detected in BJ1 hTERT G1 cells transfected with EN-T.

Supplemental Figure 4:

Compromised telomeric end-protection does not promote 53BP1 recruitment to broken telomeres. **A.** Relaxation of chromatin via treatment with trichostatin A (TSA) did not result in 53BP1 foci induction in EN-T expressing cells at any concentration. **B.** Partial depletion (siRNA knockdown) of TRF2 did not influence induction of 53BP1 foci in EN-T or TRF1 transfected BJ1hTERT cells. **C.** siRNA knockdown of TRF2 also had no measurable effect on the degree of telomere fragmentation in EJ-30 cells transfected with EN-T. **D.** shRNA knockdown of DNA-PKcs did not promote 53BP1 recruitment to telomeric DSBs in ENT transfected BJ1- hTERT cells.

Supplemental Figure 5:

Role of Apollo endonuclease in the generation of ssDNA at telomeric DSBs. **A.** While telomeric ssDNA (5'-CCCTAA-3') was slightly reduced in ENT expressing EJ-30 Apollo$^{-/-}$ G1 cells relative to ENT expressing control (wild type) EJ-30 cells, **B.** phospho-RPA32 foci were somewhat increased. Additionally, both telomeric ssDNA and phospho-RPA32 foci were increased in ENT expressing EJ-30 Apollo$^{-/-}$ S/G2 cells.